

# 1 MoS<sub>2</sub>/Epitaxial graphene layered electrodes for 2 solid-state supercapacitors

3 *Mojtaba Amjadipour*<sup>1</sup>, *Jonathan Bradford*<sup>2,3</sup>, *Negar Zebardastan*<sup>2,4</sup>, *Nunzio Motta*<sup>2,4</sup>, and  
4 *Francesca Iacopi*<sup>1,5\*</sup>

5 <sup>1</sup> School of Electrical and Data Engineering, Faculty of Engineering and Information  
6 Technology, University of Technology Sydney, NSW, Australia.

7 <sup>2</sup> School of Chemistry and Physics, Science and Engineering Faculty, Queensland University of  
8 Technology, QLD, Australia.

9 <sup>3</sup> School of Physics & Astronomy, University of Nottingham, Nottingham, NG7 2RD, United  
10 Kingdom.

11 <sup>4</sup> Centre for Materials Science, Queensland University of Technology, QLD, Australia

12 <sup>5</sup> Centre for Clean Energy Technology, University of Technology Sydney, NSW, Australia.

13 \* Corresponding author.

14 E-mail: francesca.iacopi@uts.edu.au

## 15 **Keywords**

16 quasi-solid-state supercapacitors, epitaxial graphene, MoS<sub>2</sub>, 3C-SiC

## 17 **Abstract**

18 The potential of transition metal dichalcogenides such as MoS<sub>2</sub> for energy storage has been  
19 significantly limited so far by the lack of conductivity and structural stability. Employing highly  
20 conductive, graphitic materials in combination with transition metal dichalcogenides can address  
21 this gap. Here, we explore the use of a layered electrode structure for solid-state supercapacitors,  
22 made of MoS<sub>2</sub> and epitaxial graphene on cubic silicon carbide for on-silicon energy storage. We  
23 show that the energy storage of the solid-state supercapacitors can be significantly increased by  
24 creating layered MoS<sub>2</sub>/graphene electrodes, yielding a substantial improvement as compared to

1 electrodes using either epitaxial graphene or MoS<sub>2</sub> alone. We conclude that the conductivity of  
2 epitaxial graphene and the growth morphology of MoS<sub>2</sub> on graphene play an enabling role in the  
3 successful use of transition metal dichalcogenides for on-chip energy storage.

#### 4 **1. Introduction**

5 Electrochemical supercapacitors are key components of advanced energy storage systems. Their  
6 long life cycle, low maintenance requirements, and capability to deliver high power densities make  
7 supercapacitors complementary to conventional batteries [1-6]. Charge storage in electrochemical  
8 supercapacitors relies principally on the presence of an electrical double layer at the  
9 electrode/electrolyte interface [4, 7]. Redox reactions or pseudocapacitance can also contribute to  
10 charge storage [4, 7, 8].

11 Two-dimensional transition metal sulfide (TMS) materials have recently emerged, holding, among  
12 others, high promise for energy storage applications [9-14]. These advanced layered materials  
13 present outstanding double-layer performance thanks to their high surface area and the presence  
14 of interlaminar sites for charge storage [14-18]. However, their implementation in energy storage  
15 systems has been challenged by the lack of structural stability and low conductivity [19, 20]. One  
16 of the possible ways to overcome these limitations is the combination of TMS with a material like  
17 graphene [16, 19-23]. Graphenic materials could contribute to the missing structural stability and  
18 high electrical conductivity to the thin-layered electrodes [19, 20, 24]. The efficient and scalable  
19 fabrication of graphene and TMS hybrid structures could determine the future applications of TMS  
20 materials in energy storage.

21 To date, graphene oxide (GO) and graphene flakes have been explored in combination with TMS  
22 for composite structures for energy storage applications [19, 22, 24-29]. Da Silveira Firmiano et

1 al. [19] proposed MoS<sub>2</sub>/GO composite electrodes and demonstrated that the composite structure  
2 leads to a significant capacitance performance improvement. Ji et al. [22] fabricated a flexible  
3 supercapacitor based on MoS<sub>2</sub>/GO composite electrodes using ball milling of bulk MoS<sub>2</sub> and GO  
4 powders. They demonstrated that the composite electrodes improve the capacitance by up to 50%  
5 (at 0.5 Ag<sup>-1</sup>) compared to the bulk MoS<sub>2</sub> ones [22].

6 While GO and graphene flakes provide a promising platform for flexible energy storage device  
7 fabrication [1, 22], epitaxial graphene (EG) directly grown on silicon substrates offer substantial  
8 advantages for on-chip supercapacitors [7, 30-36]. The EG on silicon technology is underpinned  
9 by a metal-based catalytic wafer-scale growth of graphene using cubic silicon carbide on silicon,  
10 which can be compatible with the current semiconductor manufacturing [31, 35, 37-41]. This  
11 binder-free method is capable of producing EG with tunable characteristics and high adhesion to  
12 the substrate, which also has the potentials for miniaturization and wafer-level production [39, 40].  
13 Pradeepkumar et al. [40] have recently demonstrated that the alloy-mediated graphitization  
14 approach maintains an epitaxial relation of graphene with the substrate; it also leads to a large area  
15 epitaxial graphene coverage. The use of layered TMS/EG electrodes for miniaturized, integrated  
16 energy storage applications **has not been investigated before**. In this study, **we explore for the first**  
17 **time** the electrochemical performance of MoS<sub>2</sub>/EG layered electrodes directly grown on a silicon  
18 substrate.

## 19 **2. Experimental methods**

### 20 2.1 Materials preparation

21 3C-SiC (cubic polytype) films epitaxially grown on Si (100) substrates have been acquired from  
22 NOVASiC. The films underwent a chemical - mechanical polishing procedure (StepSiC<sup>®</sup> by

1 NOVASIC (France)) [42, 43]. The final SiC epi layer thickness is  $\sim 500$  nm. A catalytic alloy  
2 method was employed to grow EG on the SiC films [37, 38]. A combination of a Ni layer ( $\sim 10$   
3 nm) followed by a Cu layer ( $\sim 20$  nm) was used to fabricate epitaxial graphene. A Cryopump  
4 deposition chamber operating with CD Ar<sup>+</sup> ion and 200 mA current was employed for sputtering  
5 the metallic layers. Annealing the metal-coated samples at  $\sim 1100$  °C for an hour under vacuum  
6 condition ( $\sim 10^{-5}$  mbar) leads to breaking of the Si-C bonds and the release of the carbon atoms  
7 which can form epitaxial graphene on the surface. Ni silicides are the by-product of this procedure,  
8 which were later removed with any metal residues on the surface using chemical wet etching for  
9 about nine hours (Freckle solution) [37, 38].

10 MoS<sub>2</sub> was grown by chemical vapor deposition (CVD) directly on the EG/3C-SiC/Si(100)  
11 substrates. The substrates were placed in a horizontal quartz tube furnace, 3 cm downstream from  
12 an alumina boat with 30 mg of MoO<sub>3</sub> powder. Another crucible with 1.5 g of sulfur powder was  
13 placed 20 cm upstream in a separate heating zone. Prior to the growth, the tube was pumped to  
14  $\sim 70$  Torr under 600 sccm Ar and purged for 1 hour to remove residual air. At the beginning of the  
15 growth process, the Ar flow rate was reduced to 200 sccm. The MoO<sub>3</sub> was first heated at 150 °C  
16 for 20 minutes to remove any adsorbed water, before ramping to 800 °C to evaporate the MoO<sub>3</sub>  
17 precursor. The sulfur precursor was heated simultaneously to 280 °C with a similar ramp. Both  
18 zones were held at their respective temperatures for a growth time of 20 min before cooling  
19 naturally under Ar flow.

## 20 2.2 Device fabrication

21 A sandwich cell design using two electrodes ( $\sim 2 \times 1$  cm<sup>2</sup>) with a gel electrolyte in between the  
22 electrodes was used to fabricate the quasi-solid-state supercapacitors, **as sketched in Fig.S8** [44].  
23 PVA+H<sub>2</sub>SO<sub>4</sub> gel electrolyte was prepared by mixing 1 g PVA molecule (108K molecular weight)

1 and 10 mL deionized water followed by the addition of 1g H<sub>2</sub>SO<sub>4</sub> (98%). The mixture was  
2 vigorously stirred at 80 °C for a few hours to become completely transparent. Kapton tape was  
3 used to seal the cells obtaining a typical gel electrolyte thickness of ~300 μm.

#### 4 2.3 Characterization

5 A Zeiss Supra 55VP scanning electron microscope (SEM) and Park XE7 atomic force microscope  
6 (AFM) were employed for imaging the surface. Raman spectra were collected by a WiTec Raman  
7 microscope using a 532 nm green laser; the spectra presented in this paper are obtained by  
8 averaging 2500 single spectra collected over a 100 μm<sup>2</sup> area map. X-ray photoemission  
9 spectroscopy (XPS) measurements were acquired using a Kratos Axis Supra instrument with a  
10 monochromated Al K<sub>α</sub> X-ray source (hν = 1486.7 eV).

11 An electrochemical workstation (CH Instruments, 660 E Model) was used to assess the  
12 electrochemical performance of the cells operating in a two-probe configuration. Galvanostatic  
13 charge/discharge (CD) measurements were conducted with 1 V potential window and 1-5 μA  
14 current. The stability of the cells over long cycles was assessed using the CD test over 10000 cycles  
15 by 10 μA current and 1 V potential window. The electrode areal specific capacitance was  
16 calculated based on the CD test results using the equation

$$17 \quad C = 4I\Delta t / \Delta U, \quad (1)$$

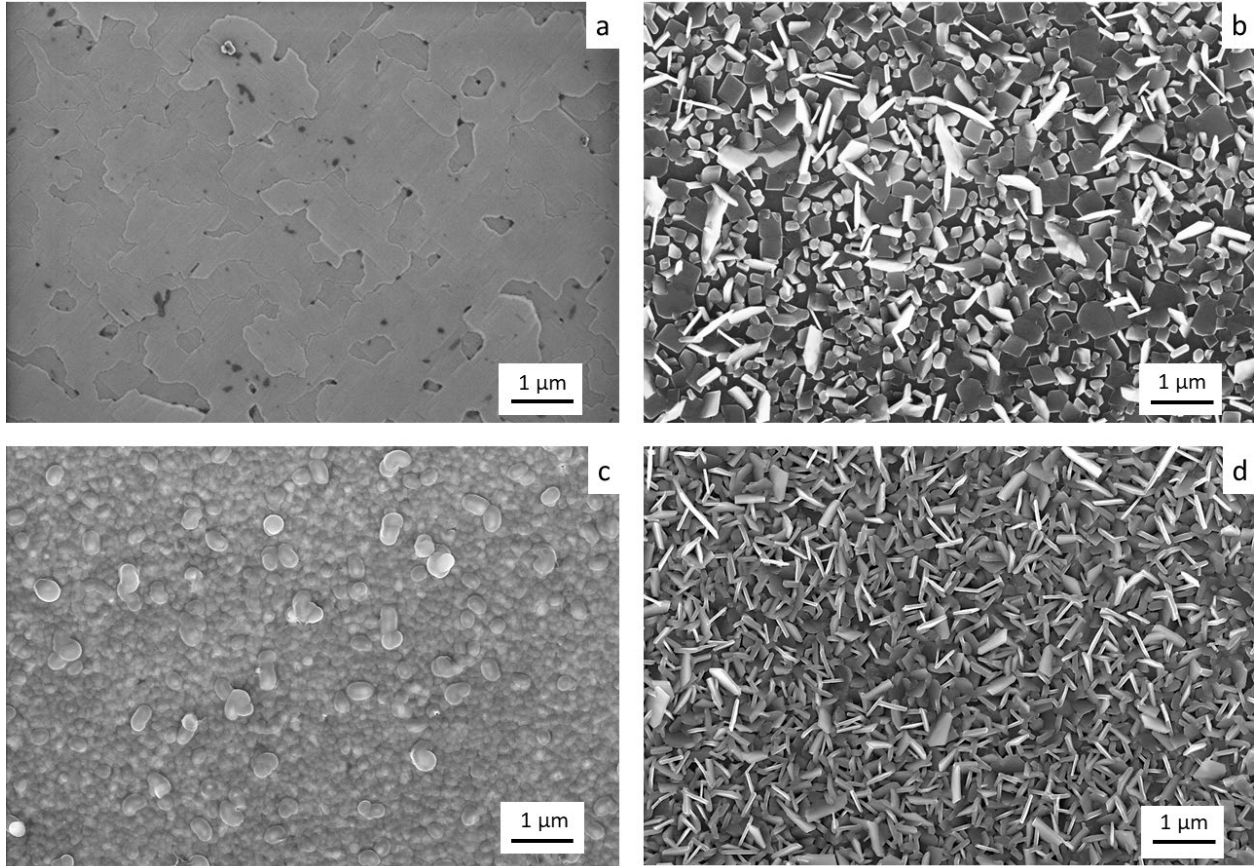
18 where C is the areal specific capacitance in (μFcm<sup>-2</sup>), I represents the current density (μAcm<sup>-2</sup>), Δt  
19 is the discharge time (s), and ΔU is the potential window (V). Data reported here are the averaged  
20 values calculated from 5 to 10 charge/discharge cycles. Electrochemical Impedance Spectroscopy  
21 measurement conducted in the 0.01 Hz to 100 kHz frequency range with a signal amplitude of 5  
22 mV.

### 1 3. Results and discussion

2 MoS<sub>2</sub> has been synthesized on two different surfaces: bare 3C-SiC/Si and EG grown on 3C-SiC/Si.  
3 **Figure 1** shows the SEM images of the samples before and after the MoS<sub>2</sub> growth. Pristine SiC  
4 presents a flat surface with a roughness root mean square (RMS) value of ~5 nm (**Figure 1a &**  
5 **S3a**), while the EG growth using the catalytic alloy method increases the roughness RMS to ~25  
6 nm (**Figure 1c & S3c**). The MoS<sub>2</sub> synthesis on both of these surfaces leads to the formation of the  
7 MoS<sub>2</sub> crystals evident in the SEM micrographs (**Figure 1b & d**). As a result, the surface roughness  
8 increases substantially in both cases after MoS<sub>2</sub> growth. The AFM measurements indicate ~44 nm  
9 RMS for the growth on bare 3C-SiC and ~54 nm RMS for the growth on EG; however, we  
10 anticipate that those values may not reflect the actual roughness of the final surfaces as the radius  
11 of curvature of the AFM tip (~30 nm) would substantially distort (**Figure S3b & d**) the  
12 morphology of the MoS<sub>2</sub> (**Figure S1a & b**). The SEM micrographs clearly indicate that the MoS<sub>2</sub>  
13 crystals grown on the EG surface are denser. Also, the MoS<sub>2</sub> tends to grow with a rather random  
14 crystal orientation on the bare SiC substrate (**Figure 1b and S1a**), while the MoS<sub>2</sub> crystals appear  
15 predominantly standing vertically on the EG surface (**Figure 1d and S1b**). The estimated  
16 thickness of grown MoS<sub>2</sub> crystals from **Figure S1b** is 30-50 nm.

17 Fei et al. [45] had illustrated the effect of the growth temperature on the orientation of the MoS<sub>2</sub>  
18 crystals, indicating that the low-temperature growth of MoS<sub>2</sub> results predominantly in a vertical  
19 alignment. The surface energy and template of the substrate used for the MoS<sub>2</sub> growth are expected  
20 to have a significant effect on the morphology of the MoS<sub>2</sub> layer as well [46-48]. Here we believe  
21 that the low surface energy of the EG layer leads to the vertical alignment of the MoS<sub>2</sub> crystals. In  
22 fact, when the growth of MoS<sub>2</sub> takes place on a defective EG surface, the MoS<sub>2</sub> layer does not

1 have the same aligned vertical orientations as seen in the high-quality EG surface, and its coverage  
2 is poor (**Figure S2**).

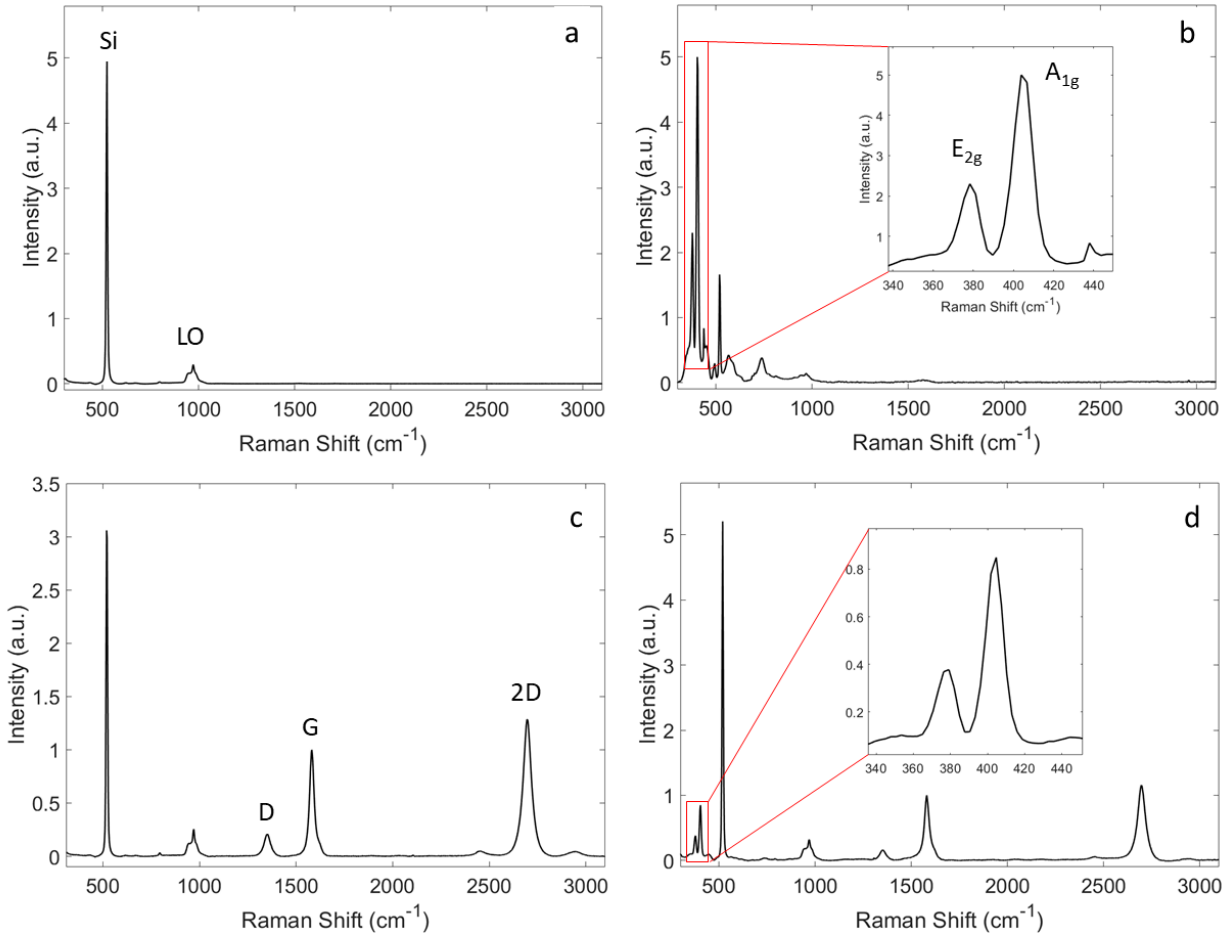


3  
4 **Figure 1.** SEM images of (a) pristine 3C-SiC/Si substrate, (b) MoS<sub>2</sub> synthesized on the 3C-SiC/Si, (c) EG  
5 grown on 3C-SiC/Si substrate, (d) MoS<sub>2</sub> grown on the EG electrodes.

6 **Figure 2a** shows the Raman spectra of the pristine 3C-SiC/Si substrate; two main notable peaks  
7 are the Si peak at  $\sim 520\text{ cm}^{-1}$  and the LO peak of SiC at  $\sim 970\text{ cm}^{-1}$  [49, 50]. After MoS<sub>2</sub> synthesis  
8 on the SiC surface, two dominant peaks E<sub>2g</sub> at  $\sim 378\text{ cm}^{-1}$  and A<sub>1g</sub> at  $\sim 404\text{ cm}^{-1}$  appear (**Figure 2b**),  
9 which correspond to in-plane and out-of-plane vibrational modes of hexagonal MoS<sub>2</sub> crystal,  
10 respectively [51, 52]. The Raman spectra of the EG sample have three extra peaks, which originate  
11 from graphene lattice: D peak at  $\sim 1340\text{ cm}^{-1}$ , G peak at  $\sim 1580\text{ cm}^{-1}$ , and 2D peak at  $\sim 2680\text{ cm}^{-1}$

1 **(Figure 2c)** [53, 54]. The D peak arises from defects within graphene lattice. The intensity ratio  
2 between D and G peaks has been widely used as a measure to compare defect density for graphene-  
3 based materials [53, 54]. The intensity ratio of  $I_{LO}/I_{2D}$  also indicates the graphene coverage over  
4 the 3C-SiC/Si substrate; lower values correspond to higher coverage. Here  $I_D/I_G$  is  $\sim 0.2$ , and  $I_{LO}/I_{2D}$   
5 is  $\sim 0.2$ , which shows the presence of good quality graphene with excellent surface coverage and  
6 low sheet resistance, as we have recently reported [40]. The Raman spectra of the EG surface after  
7 MoS<sub>2</sub> synthesis show the appearance of E<sub>2g</sub> and A<sub>1g</sub> peaks while the graphene peaks are visible,  
8 demonstrating the presence of graphene under the MoS<sub>2</sub> layer **(Figure 2d)**.  $I_D/I_G$  has appeared  
9 unchanged after MoS<sub>2</sub> growth, indicating that no significant new defects are formed during this  
10 process. However,  $I_{LO}/I_{2D}$  has increased slightly to  $\sim 0.26$ , indicating some loss of graphene **(Figure**  
11 **S5a)**. The Raman wavenumber difference between E<sub>2g</sub> and A<sub>1g</sub> peaks can be used as an indicator  
12 for assessing the number of MoS<sub>2</sub> layers [51, 55]. Here on both surfaces, the E<sub>2g</sub> and A<sub>1g</sub> peak  
13 distance is  $\sim 25 \text{ cm}^{-1}$ , corresponding to multi layers **(Figure S5b)** [51, 55]. The alignment of the  
14 MoS<sub>2</sub> crystals affects the intensity ratio of E<sub>2g</sub>/A<sub>1g</sub> peaks; the out-of-plane mode (A<sub>1g</sub>) is  
15 pronounced when the MoS<sub>2</sub> crystals are vertical due to higher exposure of the edges [56-58]. Here,  
16 the E<sub>2g</sub>/A<sub>1g</sub> ratio is higher for the MoS<sub>2</sub>/SiC electrodes (0.45) compared to the MoS<sub>2</sub>/EG (0.37),  
17 indicating that MoS<sub>2</sub> crystals are more vertically aligned on the EG surface, which is in agreement  
18 with the SEM images. This fact, along with some etching of graphene occurring during the MoS<sub>2</sub>  
19 growth, explains also the higher intensity of the Si and SiC peaks.

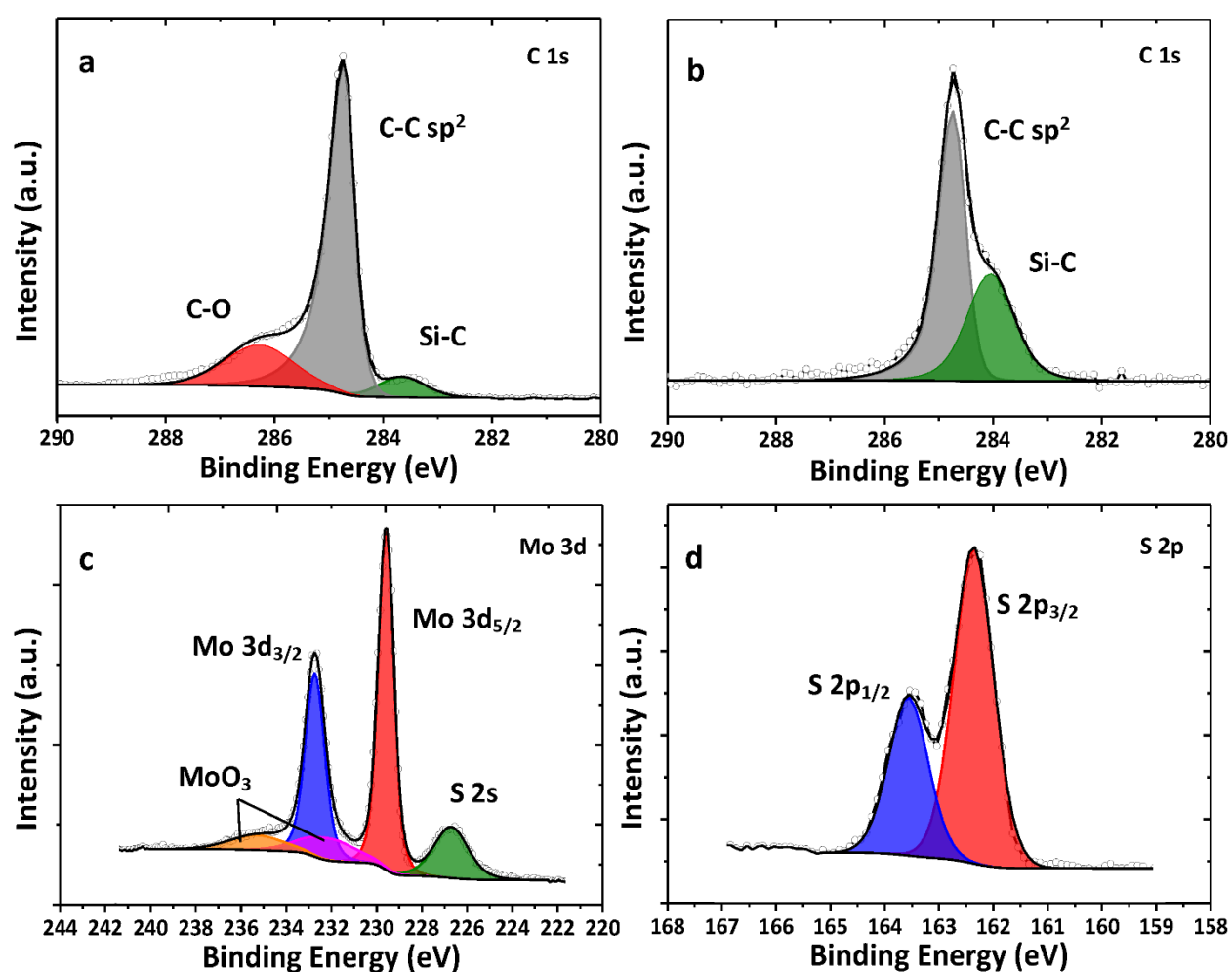




1  
 2 **Figure 2.** Raman spectra of (a) pristine 3C-SiC/Si substrate, (b) MoS<sub>2</sub> synthesized on the 3C-SiC/Si, (c)  
 3 EG grown on 3C-SiC/Si substrate, (d) MoS<sub>2</sub> synthesized on the EG electrodes.

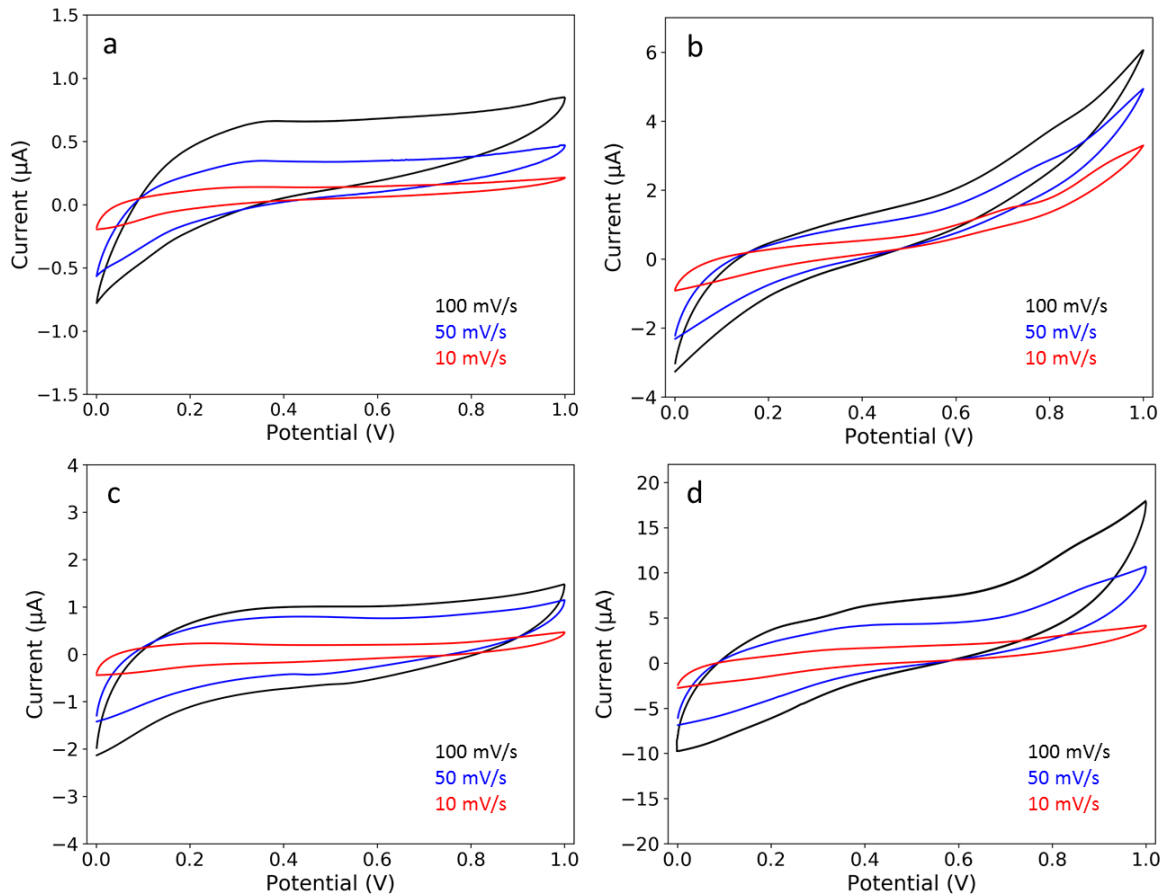
4 High-resolution XPS C 1s spectra of the EG sample show a C-C peak (attributed to graphene) at  
 5 ~284.7 eV, SiC at ~283 eV, and C-O at ~286 eV (**Figure 3a**). XPS C 1s spectra of the epitaxial  
 6 graphene sample after the MoS<sub>2</sub> synthesis show the presence of the C-C and Si-C peaks, but the  
 7 C-O peak has been removed during the MoS<sub>2</sub> growth (**Figure 3b**). We also observe that the  
 8 intensity of the C-C peak decreases after the MoS<sub>2</sub> growth. Specifically, the ratio of the intensities  
 9 of the C-C and Si-C peaks decreases by a factor of ~ 6, which indicates that some graphene has  
 10 been etched away during the growth process. This is in agreement with the I<sub>LO</sub>/I<sub>2D</sub> increase  
 11 observed in the Raman measurements. Mo XPS 3d spectra show two intense peaks of Mo 3d<sub>5/2</sub>

1 (~228 eV) and Mo 3d<sub>3/2</sub> (~231.2 eV), which relate to the Mo (IV) oxidation state of MoS<sub>2</sub>, while  
 2 the less intense peak at ~225.2 eV corresponds to S 2s of MoS<sub>2</sub> (**Figure 3c**) [59]. A less intense  
 3 doublet at ~231.2/233.8 eV corresponds to the Mo (VI) oxidation state in MoO<sub>3</sub>, attributed to some  
 4 residual oxide present on the surface after MoS<sub>2</sub> growth. The S 2p region indicates the presence of  
 5 two peaks, S 2p<sub>3/2</sub> (~160.6 eV) and S 2p<sub>1/2</sub> (~162.1 eV), which are characteristic of the Mo-S  
 6 bonding (**Figure 3d**) [59].



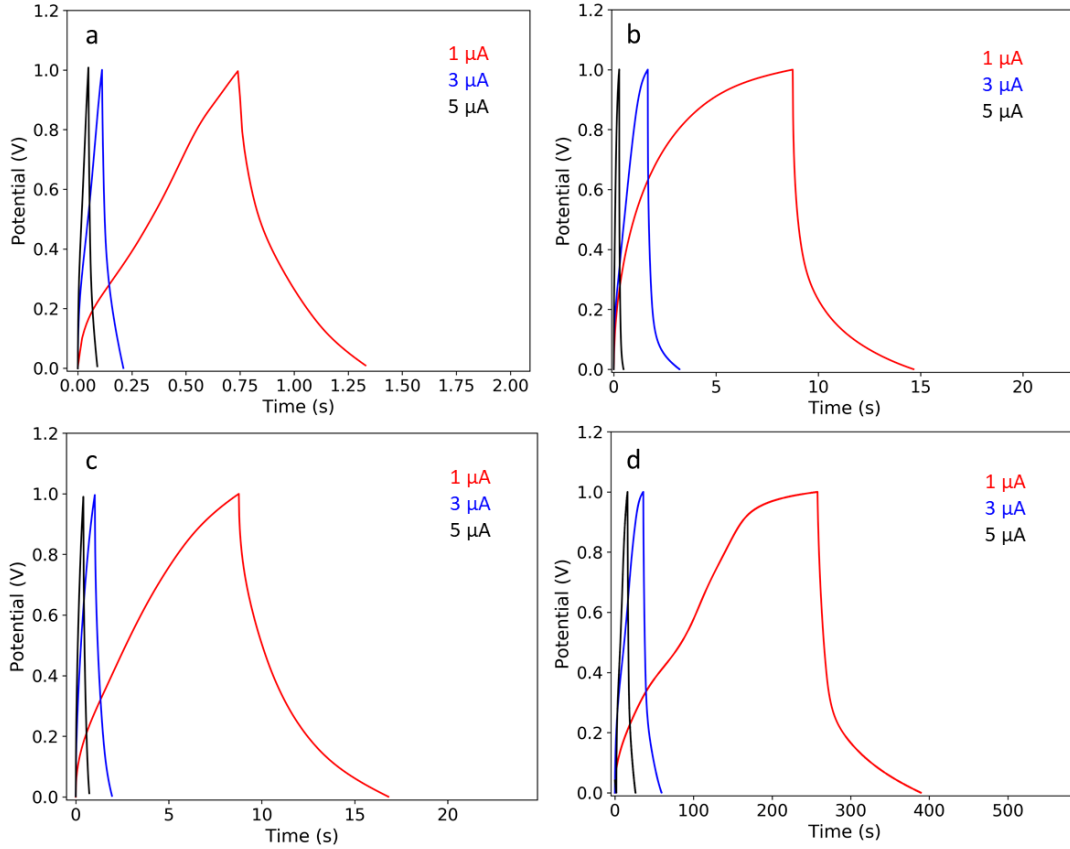
7  
 8 **Figure 3.** XPS C 1s spectra of (a) EG/3C-SiC/Si, (b) after MoS<sub>2</sub> synthesis. (c) Mo 3d spectra of the electrode  
 9 after MoS<sub>2</sub> synthesis, (d) S 2p spectra of the same sample.

1 The CV curve of the cells fabricated with the bare 3C-SiC/Si electrodes shows a quasi-rectangular  
2 shape, which is characteristic of double-layer charge storage (**Figure 4a**). The CV tests of the cell  
3 with MoS<sub>2</sub>/3C-SiC electrodes show a minor improvement in capacitance (**Figure 4b**) compared  
4 to the 3C-SiC/Si cell as the area enclosed by the curve is indicative of the charge storage capacity.  
5 The CV curves of the cell fabricated using MoS<sub>2</sub>/EG hybrid electrodes demonstrate a significant  
6 improvement in charge storage, with a more than six-fold increase in the area (**Figure d**).  
7 Particularly, the importance of graphene for harnessing the MoS<sub>2</sub> energy storage capabilities  
8 becomes evident when comparing the CV test results of the cell fabricated with MoS<sub>2</sub>/3C-SiC  
9 electrodes with the MoS<sub>2</sub>/EG ones (**Figure 4b & d**).



1 **Figure 4.** CV curves of the cells fabricated with (a) pristine 3C-SiC/Si, (b) MoS<sub>2</sub> synthesized on the 3C-  
2 SiC/Si, (c) EG grown on 3C-SiC/Si, (d) MoS<sub>2</sub> synthesized on the EG. All the CV curves are presented on  
3 the same scale to help the comparison. The vertical range in panel d is 5 times that of panel b and c, and 12  
4 times that of panel a, demonstrating the large increase in efficiency.

5 **Figure 5** shows the galvanostatic charge/discharge test results of the cells, and table 1 presents the  
6 electrodes' areal specific capacitance calculated based on the charge/discharge test results. The  
7 bare 3C-SiC electrodes yield the smallest capacitance. The capacitance of the electrodes made of  
8 MoS<sub>2</sub> alone on 3C-SiC (no EG) does not show substantial improvement. However, the cell with  
9 electrodes of MoS<sub>2</sub> coupled with EG on 3C-SiC yields a remarkable increase in areal capacitance,  
10 from 24 μF/cm<sup>2</sup> to 554 μF/cm<sup>2</sup> at 1 μA (**Table 1**). The energy densities (E) are estimated using  
11 the relationship  $E = \frac{1}{2} C (\Delta U)^2$ . It is interesting to note that although the MoS<sub>2</sub>/3C-SiC electrodes  
12 offer a significantly higher surface area compared to the EG only electrodes, they show lower  
13 capacitance. This indicates the importance of electrode conductivity in charge storage applications  
14 of TMS materials. Electrochemical impedance spectroscopy measurement data also indicates that  
15 MoS<sub>2</sub>/EG electrodes have lower impedance, as expected, compared to MoS<sub>2</sub>/3C-SiC electrodes  
16 (**Figure S6**). This improvement of the electrode/electrolyte interface impedance has a beneficial  
17 effect on the capacitance performance, as seen from the CV and CD data. Having said that, the  
18 vertical alignment of the MoS<sub>2</sub> nanosheets on the EG surface drastically limits the total contact  
19 area of each MoS<sub>2</sub> with graphene, slowing down charging and charge collection processes at the  
20 interface of the two materials. We expect this factor to be a possible reason for the observed  
21 distortion in the charge/discharge curves. This hypothesis is corroborated by the fact that the  
22 distortion is very pronounced for the cells containing MoS<sub>2</sub> (**Figure 5b and d**), particularly for the  
23 MoS<sub>2</sub> on EG cells (**Figure 5d**), where most of the crystals are indeed vertically aligned.



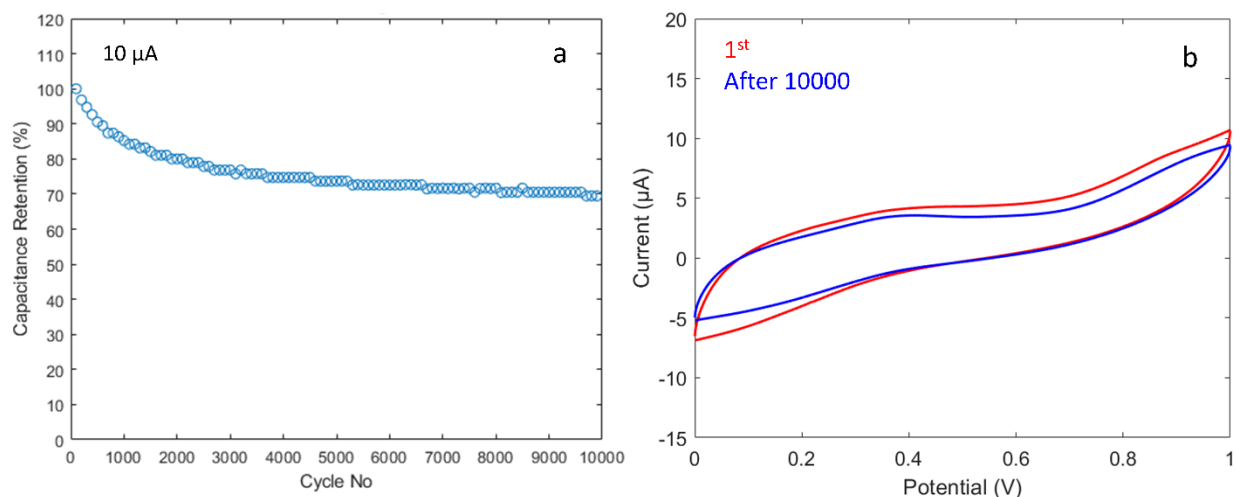
1  
 2 **Figure 5.** Galvanostatic charge/discharge test result of the cells fabricated with (a) pristine 3C-SiC/Si, (b)  
 3 MoS<sub>2</sub> synthesized on the 3C-SiC/Si, (c) EG grown on 3C-SiC/Si, (d) MoS<sub>2</sub> synthesized on the EG.  
 4 **Table 1.** The electrodes' specific capacitance calculated from galvanostatic charge/discharge tests and  
 5 their corresponding energy densities.

Electrode Type	I (μA)	Electrode Type			
		SiC/Si	MoS <sub>2</sub> /SiC/Si	Epitaxial Graphene	MoS <sub>2</sub> /Epitaxial Graphene
C (μF/cm <sup>2</sup> )	1	2.5	24	32	554
	3	1.2	18	11	275
	5	1	4	7	190
E (μWh/m <sup>2</sup> )	1	3.5	33.3	44.4	769.4
	3	1.7	25	15.3	381.9
	5	1.4	5.6	9.7	263.9

1

2 The best performing cell, made of MoS<sub>2</sub>/EG hybrid electrodes, has been further tested for long  
3 cycling charge/discharge. **Figure 6** indicates that the MoS<sub>2</sub>/EG electrodes tend to drop about 30%  
4 of their performance over 10000 cycles. The capacitance drops by 20% after 2000 cycles, and it  
5 only drops further 10% after 8000 cycles (**Figure 6a**). Such retention drop has also been reported  
6 for the MoS<sub>2</sub>/reduced graphene oxide composite electrodes [11, 20, 60]. However, note that the  
7 CV tests of the cell in the initial condition and after 10000 cycles of charge/discharge does not  
8 show a significant performance change (**Figure 6b**).

9



10

11 **Figure 6.** (a) Long cycling galvanostatic charge/discharge test result of the cell fabricated with MoS<sub>2</sub>/EG  
12 hybrid electrodes, (b) CV curves with 50 mV/s scan rate of the cell at the initial condition and after 10000  
13 charge/discharge tests.

14 Finally, it should be noted that defective graphenic material is generally superior to low-defect  
15 graphene as an electrode for supercapacitors, being more chemically active and providing a higher  
16 amount of charge storage sites [8, 41, 44]. However, a highly defective graphenic layer is not  
17 efficient in combination with MoS<sub>2</sub> (**Figure S2 and S7**), because of the lack of a highly conductive

1 medium. When used in combination with MoS<sub>2</sub>, a highly-conductive and low-defect graphene is  
2 necessary to complement the MoS<sub>2</sub> capabilities for energy storage.

3

#### 4 **4. Conclusions**

5 In summary, we have shown that epitaxial graphene on cubic silicon carbide can complement well  
6 the use of transition metal sulfides for miniaturized, on-chip supercapacitors. Epitaxial graphene  
7 provides a highly conductive medium for the MoS<sub>2</sub> layer leading to a capacitance improvement of  
8 more than 20 times, as compared to electrodes made of MoS<sub>2</sub> alone. A graphene layer with good  
9 coverage and low-defect density is key for enabling the charge storage capabilities of the MoS<sub>2</sub>  
10 layer. In addition, the epitaxial graphene surface provides a template for prevalently vertical  
11 growth of MoS<sub>2</sub> crystals, which also increases the total accessible and active area for energy  
12 storage. On the other hand, the vertical alignment of the crystals also limits the contact surface  
13 between MoS<sub>2</sub> and graphene, slowing down the charging and charge collection at the interface.  
14 We believe that further tuning of the TMS growth temperature could lead to the improvement of  
15 the growth orientation achieving a trade-off between an increase in capacitance and responsivity  
16 of the system, according to the specific final application.

17 These insights offer a new path to develop further miniaturized on-chip energy storage systems  
18 compatible with silicon electronics based on layered materials, which can support the power  
19 demand to operate integrated smart systems.

## 1   **ACKNOWLEDGMENT**

2   Funding from the Air Force Office for Scientific Research through grant 18IOA052 and from ARC  
3   through the Discovery Project DP200102546 is kindly acknowledged. The UTS MAU labs are  
4   acknowledged for providing access to the fabrication facilities. This work was also enabled by the  
5   Central Analytical Research Facility hosted by the Institute for Future Environments at QUT.

6

## 7   **REFERENCES**

- 8   [1] Z. Niu, L. Zhang, L. Liu, B. Zhu, H. Dong, X. Chen, All - solid - state flexible ultrathin  
9   micro - supercapacitors based on graphene, *Advanced Materials*, 25 (2013) 4035-4042.
- 10   [2] C.-H. Chang, B. Hsia, J.P. Alper, S. Wang, L.E. Luna, C. Carraro, S.-Y. Lu, R. Maboudian,  
11   High-temperature all solid-state microsupercapacitors based on SiC nanowire electrode and YSZ  
12   electrolyte, *ACS Applied Materials & Interfaces*, 7 (2015) 26658-26665.
- 13   [3] J. Li, S. Sollami Delekta, P. Zhang, S. Yang, M.R. Lohe, X. Zhuang, X. Feng, M. Östling,  
14   Scalable fabrication and integration of graphene microsupercapacitors through full inkjet  
15   printing, *ACS Nano*, 11 (2017) 8249-8256.
- 16   [4] J. Liang, A.K. Mondal, D.-W. Wang, F. Iacopi, Graphene-based planar microsupercapacitors:  
17   recent advances and future challenges, *Advanced Materials Technologies*, 4 (2019) 1800200.
- 18   [5] E. Frackowiak, F. Beguin, Carbon materials for the electrochemical storage of energy in  
19   capacitors, *Carbon*, 39 (2001) 937-950.
- 20   [6] Y. Zhao, J. Liu, B. Wang, J. Sha, Y. Li, D. Zheng, M. Amjadipour, J. MacLeod, N. Motta,  
21   Supercapacitor electrodes with remarkable specific capacitance converted from hybrid graphene  
22   Oxide/NaCl/Urea Films, *ACS Applied Materials & Interfaces*, 9 (2017) 22588-22596.
- 23   [7] M. Conte, Supercapacitors technical requirements for new applications, *Fuel Cells*, 10 (2010)  
24   806-818.
- 25   [8] M. Amjadipour, D. Su, F. Iacopi, Graphitic-based solid-state supercapacitors: enabling redox  
26   reaction by in situ electrochemical treatment, *Batteries & Supercaps*, 3 (2020).
- 27   [9] J.M. Soon, K.P. Loh, Electrochemical double-layer capacitance of MoS<sub>2</sub> nanowall films,  
28   *Electrochemical and Solid-State Letters*, 10 (2007) A250-A254.
- 29   [10] L. Cao, S. Yang, W. Gao, Z. Liu, Y. Gong, L. Ma, G. Shi, S. Lei, Y. Zhang, S. Zhang,  
30   Direct laser - patterned micro - supercapacitors from paintable MoS<sub>2</sub> films, *Small*, 9 (2013)  
31   2905-2910.



- 1 [11] T. Wang, S. Chen, H. Pang, H. Xue, Y. Yu, MoS<sub>2</sub> - based nanocomposites for  
2 electrochemical energy storage, *Advanced Science*, 4 (2017) 1600289.
- 3 [12] P. Sun, R. Wang, Q. Wang, H. Wang, X. Wang, Uniform MoS<sub>2</sub> nanolayer with sulfur  
4 vacancy on carbon nanotube networks as binder-free electrodes for asymmetrical supercapacitor,  
5 *Applied Surface Science*, 475 (2019) 793-802.
- 6 [13] L. Wang, Y. Ma, M. Yang, Y. Qi, Titanium plate supported MoS<sub>2</sub> nanosheet arrays for  
7 supercapacitor application, *Applied Surface Science*, 396 (2017) 1466-1471.
- 8 [14] H. Sun, H. Liu, Z. Hou, R. Zhou, X. Liu, J.-G. Wang, Edge-terminated MoS<sub>2</sub> nanosheets  
9 with an expanded interlayer spacing on graphene to boost supercapacitive performance, *Chemical*  
10 *Engineering Journal*, 387 (2020) 124204.
- 11 [15] Y.-T. Liu, X.-D. Zhu, Z.-Q. Duan, X.-M. Xie, Flexible and robust MoS<sub>2</sub>-graphene hybrid  
12 paper cross-linked by a polymer ligand: a high-performance anode material for thin film lithium-  
13 ion batteries, *Chemical Communications*, 49 (2013) 10305-10307.
- 14 [16] H. Wang, H. Feng, J. Li, Graphene and graphene - like layered transition metal  
15 dichalcogenides in energy conversion and storage, *Small*, 10 (2014) 2165-2181.
- 16 [17] D. Sarkar, D. Das, S. Das, A. Kumar, S. Patil, K.K. Nanda, D.D. Sarma, A. Shukla,  
17 Expanding Interlayer Spacing in MoS<sub>2</sub> for Realizing an Advanced Supercapacitor, *ACS Energy*  
18 *Letters*, 4 (2019) 1602-1609.
- 19 [18] M. Acerce, D. Voiry, M. Chhowalla, Metallic 1T phase MoS<sub>2</sub> nanosheets as supercapacitor  
20 electrode materials, *Nature Nanotechnology*, 10 (2015) 313-318.
- 21 [19] E.G. da Silveira Firmiano, A.C. Rabelo, C.J. Dalmaschio, A.N. Pinheiro, E.C. Pereira, W.H.  
22 Schreiner, E.R. Leite, Supercapacitor electrodes obtained by directly bonding 2D MoS<sub>2</sub> on  
23 reduced graphene oxide, *Advanced Energy Materials*, 4 (2014) 1301380.
- 24 [20] X. Xie, Z. Ao, D. Su, J. Zhang, G. Wang, MoS<sub>2</sub>/Graphene composite anodes with enhanced  
25 performance for sodium - ion batteries: the role of the two - dimensional heterointerface,  
26 *Advanced Functional Materials*, 25 (2015) 1393-1403.
- 27 [21] P. Geng, S. Zheng, H. Tang, R. Zhu, L. Zhang, S. Cao, H. Xue, H. Pang, Transition metal  
28 sulfides based on graphene for electrochemical energy storage, *Advanced Energy Materials*, 8  
29 (2018) 1703259.
- 30 [22] H.-M. Ji, A.-L. Luan, C.-C. Dai, M. Li, G. Yang, W.-H. Hou, Highly active free-standing  
31 and flexible MoS<sub>2</sub>/rGO sandwich-structured films for supercapacitor applications, *Solid State*  
32 *Communications*, 297 (2019) 45-49.
- 33 [23] H.-U. Kim, M. Kim, Y. Jin, Y. Hyeon, K.S. Kim, B.-S. An, C.-W. Yang, V. Kanade, J.-Y.  
34 Moon, G.Y. Yeom, Low-temperature wafer-scale growth of MoS<sub>2</sub>-graphene heterostructures,  
35 *Applied Surface Science*, 470 (2019) 129-134.
- 36 [24] J. Li, K. Liao, X. Wang, P. Shi, J. Fan, Q. Xu, Y. Min, High - Performance Flexible All -  
37 Solid - State Supercapacitors Based on Ultralarge Graphene Nanosheets and Solvent -  
38 Exfoliated Tungsten Disulfide Nanoflakes, *Advanced Materials Interfaces*, 4 (2017) 1700419.

- 1 [25] N. Li, T. Lv, Y. Yao, H. Li, K. Liu, T. Chen, Compact graphene/MoS<sub>2</sub> composite films for  
2 highly flexible and stretchable all-solid-state supercapacitors, *Journal of Materials Chemistry A*,  
3 5 (2017) 3267-3273.
- 4 [26] M.A. Bissett, I.A. Kinloch, R.A. Dryfe, Characterization of MoS<sub>2</sub>-graphene composites for  
5 high-performance coin cell supercapacitors, *ACS Applied Materials & Interfaces*, 7 (2015)  
6 17388-17398.
- 7 [27] F. Clerici, M. Fontana, S. Bianco, M. Serrapede, F. Perrucci, S. Ferrero, E. Tresso, A.  
8 Lamberti, In situ MoS<sub>2</sub> decoration of laser-induced graphene as flexible supercapacitor  
9 electrodes, *ACS Applied Materials & Interfaces*, 8 (2016) 10459-10465.
- 10 [28] H. Ji, S. Hu, Z. Jiang, S. Shi, W. Hou, G. Yang, Directly scalable preparation of sandwiched  
11 MoS<sub>2</sub>/graphene nanocomposites via ball-milling with excellent electrochemical energy storage  
12 performance, *Electrochimica Acta*, 299 (2019) 143-151.
- 13 [29] M. Saraf, K. Natarajan, S.M. Mobin, Emerging Robust Heterostructure of MoS<sub>2</sub>-rGO for  
14 High-Performance Supercapacitors, *ACS Applied Materials & Interfaces*, 10 (2018) 16588-  
15 16595.
- 16 [30] M. Amjadipour, A. Tadich, J.J. Boeckl, J. Lipton-Duffin, J. MacLeod, F. Iacopi, N. Motta,  
17 Quasi free-standing epitaxial graphene fabrication on 3C-SiC/Si(111), *Nanotechnology*, 29  
18 (2018) 145601.
- 19 [31] N. Mishra, J. Boeckl, N. Motta, F. Iacopi, Graphene growth on silicon carbide: a review,  
20 *Physica Status Solidi (a)*, 213 (2016) 2277-2289.
- 21 [32] C. Riedl, C. Coletti, U. Starke, Structural and electronic properties of epitaxial graphene on  
22 SiC (0 0 0 1): a review of growth, characterization, transfer doping and hydrogen intercalation,  
23 *Journal of Physics D: Applied Physics*, 43 (2010) 374009.
- 24 [33] W.A. De Heer, C. Berger, M. Ruan, M. Sprinkle, X. Li, Y. Hu, B. Zhang, J. Hankinson, E.  
25 Conrad, Large area and structured epitaxial graphene produced by confinement controlled  
26 sublimation of silicon carbide, *Proceedings of the National Academy of Sciences*, 108 (2011)  
27 16900-16905.
- 28 [34] S. Wang, B. Hsia, C. Carraro, R. Maboudian, High-performance all solid-state micro-  
29 supercapacitor based on patterned photoresist-derived porous carbon electrodes and an ionogel  
30 electrolyte, *Journal of Materials Chemistry A*, 2 (2014) 7997-8002.
- 31 [35] F. Liu, A. Gutes, I. Laboriante, C. Carraro, R. Maboudian, Graphitization of n-type  
32 polycrystalline silicon carbide for on-chip supercapacitor application, *Applied Physics Letters*,  
33 99 (2011) 112104.
- 34 [36] B. Hsia, M.S. Kim, M. Vincent, C. Carraro, R. Maboudian, Photoresist-derived porous  
35 carbon for on-chip micro-supercapacitors, *Carbon*, 57 (2013) 395-400.
- 36 [37] F. Iacopi, N. Mishra, B.V. Cuning, D. Goding, S. Dimitrijevic, R. Brock, R.H. Dauskardt, B.  
37 Wood, J. Boeckl, A catalytic alloy approach for graphene on epitaxial SiC on silicon wafers,  
38 *Journal of Materials Research*, 30 (2015) 609-616.
- 39 [38] N. Mishra, J.J. Boeckl, A. Tadich, R.T. Jones, P.J. Pigram, M. Edmonds, M.S. Fuhrer, B.M.  
40 Nichols, F. Iacopi, Solid source growth of graphene with Ni-Cu catalysts: towards high quality  
41 in situ graphene on silicon, *Journal of Physics D: Applied Physics*, 50 (2017) 095302.

- 1 [39] B.V. Cunning, M. Ahmed, N. Mishra, A.R. Kermany, B. Wood, F. Iacopi, Graphitized  
2 silicon carbide microbeams: wafer-level, self-aligned graphene on silicon wafers,  
3 *Nanotechnology*, 25 (2014) 325301.
- 4 [40] A. Pradeepkumar, M. Amjadipour, N. Mishra, C. Liu, M.S. Fuhrer, A. Bendavid, F. Isa, M.  
5 Zielinski, H.I. Sirikumara, T. Jayasekara, D.K. Gaskill, F. Iacopi, p-type epitaxial graphene on  
6 cubic silicon carbide on silicon for integrated silicon technologies, *ACS Applied Nano Materials*,  
7 3 (2019) 830-841.
- 8 [41] M. Ahmed, B. Wang, B. Gupta, J.J. Boeckl, N. Motta, F. Iacopi, On-silicon supercapacitors  
9 with enhanced storage performance, *Journal of The Electrochemical Society*, 164 (2017) A638-  
10 A644.
- 11 [42] M. Portail, M. Zielinski, T. Chassagne, S. Roy, M. Nemoz, Comparative study of the role of  
12 the nucleation stage on the final crystalline quality of (111) and (100) silicon carbide films  
13 deposited on silicon substrates, *Journal of Applied Physics*, 105 (2009) 083505.
- 14 [43] G. Chichignoud, M. Ucar-Morais, M. Pons, E. Blanquet, Chlorinated silicon carbide CVD  
15 revisited for polycrystalline bulk growth, *Surface and Coatings Technology*, 201 (2007) 8888-  
16 8892.
- 17 [44] B. Wang, M. Ahmed, B. Wood, F. Iacopi, All-solid-state supercapacitors on silicon using  
18 graphene from silicon carbide, *Applied Physics Letters*, 108 (2016) 183903.
- 19 [45] L. Fei, S. Lei, W.-B. Zhang, W. Lu, Z. Lin, C.H. Lam, Y. Chai, Y. Wang, Direct TEM  
20 observations of growth mechanisms of two-dimensional MoS<sub>2</sub> flakes, *Nature Communications*,  
21 7 (2016) 1-7.
- 22 [46] P. Yang, S. Zhang, S. Pan, B. Tang, Y. Liang, X. Zhao, Z. Zhang, J. Shi, Y. Huan, Y. Shi,  
23 Epitaxial growth of centimeter-scale single-crystal MoS<sub>2</sub> monolayer on Au (111), *ACS Nano*, 14  
24 (2020) 5036-5045.
- 25 [47] K.V. Bets, N. Gupta, B.I. Yakobson, How the complementarity at vicinal steps enables  
26 growth of 2D monocrystals, *Nano letters*, 19 (2019) 2027-2031.
- 27 [48] J. Sitek, J. Plochanski, I. Pasternak, A.P. Gertych, C. McAleese, B.R. Conran, M. Zdrojek,  
28 W. Strupinski, Substrate-induced variances in morphological and structural properties of MoS<sub>2</sub>  
29 grown by chemical vapor deposition on epitaxial graphene and SiO<sub>2</sub>, *ACS Applied Materials &*  
30 *Interfaces*, (2020).
- 31 [49] F. Iacopi, G. Walker, L. Wang, L. Malesys, S. Ma, B.V. Cunning, A. Iacopi, Orientation-  
32 dependent stress relaxation in hetero-epitaxial 3C-SiC films, *Applied Physics Letters*, 102 (2013)  
33 011908.
- 34 [50] B. Gupta, M. Notarianni, N. Mishra, M. Shafiei, F. Iacopi, N. Motta, Evolution of epitaxial  
35 graphene layers on 3C SiC/Si (111) as a function of annealing temperature in UHV, *Carbon*, 68  
36 (2014) 563-572.
- 37 [51] C. Lee, H. Yan, L.E. Brus, T.F. Heinz, J. Hone, S. Ryu, Anomalous lattice vibrations of  
38 single-and few-layer MoS<sub>2</sub>, *ACS Nano*, 4 (2010) 2695-2700.
- 39 [52] K. Wang, J. Wang, J. Fan, M. Lotya, A. O'Neill, D. Fox, Y. Feng, X. Zhang, B. Jiang, Q.  
40 Zhao, Ultrafast saturable absorption of two-dimensional MoS<sub>2</sub> nanosheets, *ACS Nano*, 7 (2013)  
41 9260-9267.

- 1 [53] L. Malard, M. Pimenta, G. Dresselhaus, M. Dresselhaus, Raman spectroscopy in graphene,  
2 Physics Reports, 473 (2009) 51-87.
- 3 [54] A.C. Ferrari, Raman spectroscopy of graphene and graphite: disorder, electron-phonon  
4 coupling, doping and nonadiabatic effects, Solid State Communications, 143 (2007) 47-57.
- 5 [55] J. Jeon, S.K. Jang, S.M. Jeon, G. Yoo, Y.H. Jang, J.-H. Park, S. Lee, Layer-controlled CVD  
6 growth of large-area two-dimensional MoS<sub>2</sub> films, Nanoscale, 7 (2015) 1688-1695.
- 7 [56] Y. Jung, J. Shen, Y. Liu, J.M. Woods, Y. Sun, J.J. Cha, Metal seed layer thickness-induced  
8 transition from vertical to horizontal growth of MoS<sub>2</sub> and WS<sub>2</sub>, Nano Letters, 14 (2014) 6842-  
9 6849.
- 10 [57] D. Kong, H. Wang, J.J. Cha, M. Pasta, K.J. Koski, J. Yao, Y. Cui, Synthesis of MoS<sub>2</sub> and  
11 MoSe<sub>2</sub> films with vertically aligned layers, Nano Letters, 13 (2013) 1341-1347.
- 12 [58] F. Lan, Z. Lai, Y. Xu, H. Cheng, Z. Wang, C. Qi, J. Chen, S. Zhang, Synthesis of vertically  
13 standing MoS<sub>2</sub> triangles on SiC, Scientific Reports, 6 (2016) 1-5.
- 14 [59] N. Turner, A. Single, Determination of peak positions and areas from wide - scan XPS  
15 spectra, Surface and Interface Analysis, 15 (1990) 215-222.
- 16 [60] K. Chang, W. Chen, L-cysteine-assisted synthesis of layered MoS<sub>2</sub>/graphene composites  
17 with excellent electrochemical performances for lithium ion batteries, ACS Nano, 5 (2011) 4720-  
18 4728.
- 19